Controlling of Structural Ordering and Rigidity of β-SiAlON:Eu through Chemical Cosubstitution to Approach Narrow-Band-Emission for Light-Emitting Diodes Application

Xuejie Zhang,[†] Mu-Huai Fang,[†] Yi-Ting Tsai,[†] Agata Lazarowska,[*,∥] Sebastian Mahlik,[∥] Tadeusz Lesniewski,[∥] Marek Grinberg,[∥] Wei Kong Pang,[@] Fengjuan Pan,[‡] Chaolun Liang,[#] Wuzong Zhou,[#] Jing Wang,[φ] Jyh-Fu Lee,[§] Bing-Ming Cheng,[§] Tsu-Lien Hung,[∞] Yang-Yuan Chen,[∞] and Ru-Shi Liu[*,†,£]

[†]Department of Chemistry, National Taiwan University, Taipei 106, Taiwan

[∥]Institute of Experimental Physics, Faculty of Mathematics, Physics and Informatics, University of Gdańsk, 80-308 Gdańsk, Poland

[@]Institute for Superconducting & Electronic Materials, University of Wollongong, NSW 2522, Australia

[‡]College of Chemistry and Molecular Engineering, Peking University, Beijing 100871, China

[#]EaStCHEM, School of Chemistry, University of St Andrews, St Andrews, Fife KY16 9ST, United Kingdom

[φ]School of Chemistry, Sun Yat-sen University, Guangzhou 510275, China

[§]National Synchrotron Radiation Research Center, Hsinchu 300, Taiwan

[∞]Institute of Physics, Academia Sinica, Taipei 11529, Taiwan

[£]Department of Mechanical Engineering and Graduate Institute of Manufacturing Technology, National Taipei University of Technology, Taipei 106, Taiwan

ABSTRACT: Narrow-band green-emitting phosphor β-SiAlON:Eu has been widely used in advanced wide-gamut backlighting devices. However, the origins for unusual sharp lines in photoluminescence emission at room temperature and tunable narrow-band-emission tailored by reducing Al-O in β-SiAlON:Eu are still unclear. Here, the presence of sharp-line fine structure in the emission spectra of β-SiAlON:Eu is mainly due to purely electronic transitions (zero phonon lines) and their vibronic repetitions resulted from the multi-microenvironment around Eu^{2+} ions that has been revealed by relative emission intensity of sharp line depends on excitation wavelength and monotonously increasing decay time. The specific features of the Eu^{2+} occupying interstitial sites indicate that the effect of crystal field strength can be neglected. Therefore the enhanced rigidity and higher ordering structure of β-SiAlON:Eu with decreasing the substitution of Si–N by Al–O become the main factors in decreasing electron–lattice coupling and reducing inhomogeneous broadening, favouring the blue-shift and narrow of the emission band, the enhanced thermal stability, as well as the charge state of Eu^{2+}. Our results provide new insights for explaining the reason for narrow-band-emission in β-SiAlON:Eu, which will deliver an impetus for the exploration of phosphors with narrow band and ordering structure.

1. INTRODUCTION

To obtain the maximum accessible color gamut of LCD displays employing phosphor-converted white LEDs as backlighting, a solid-state material with narrower green-emission bandwidth is urgently to be explored.[1–4] To date, β-SiAlON:Eu, as the state-of-the-art green phosphor, is widely applied to fabricate advanced wide-gamut backlighting device due to its favourable properties, such as narrow emission bandwidth (45–55 nm), excellent thermal quenching behavior (~10% emission loss at 150 °C), and high external quantum efficiency. However, the origin of narrow-band-emission in β-SiAlON:Eu and the underlying reason for tunable photoluminescence through replacing Si–N by Al–O remains under debate.[5,6] β-SiAlON is structurally derived from β-Si_3N_4 via equivalent substitution of Si–N by Al–O, leading to a formula of β-$Si_{6-z}Al_zO_zN_{8-z}$ ($0 < z \leq 4.2$), where z represents the number of Al–O pairs substituting for Si–N pairs.[7–11] Hirosaki[12] *et al.* reported for the first time a Eu doped β-SiAlON green phosphor, which has an emission peak at 535 nm with a full width at half maximum (FWHM) of 55 nm. However, due to the effective ionic radii of Eu^{2+} (6CN, 1.17 Å) being much larger than that of Al^{3+} (6CN, 0.535 Å) and Si^{4+} (6CN, 0.400 Å), it is impossible for Eu^{2+} to occupy the sites of Al^{3+} and Si^{4+}. Persistent effort has been devoted to determining the microenvironment of Eu^{2+} ions using conventional structural analysis techniques, but it is still a pending issue because the doped content of Eu in β-SiAlON lattice is too small. A homogeneous distribution of Eu^{2+} in β-SiAlON particle was observed,[12] which demonstrated that Eu^{2+} was probably occupied at a specific atomic site, such as the channels along the c axis. Based on this, Kimoto[13] *et al.* directly observed a single

Eu dopant atom in β-SiAlON using scanning transmission electron microscopy (STEM) and revealed that Eu ion exists in a continuous atomic channel in the β-SiAlON structure. Recently, Wang[14] *et al.* found that Eu^{2+} is coordinated by nine nitrogen atoms, forming a highly symmetric EuN_9 polyhedron because of Eu^{2+}, within the same plane as the Al and O atoms, having minimum stable energy. To date, in β-SiAlON:Eu, the consensus is that a single crystallographic site existed in the highly symmetric hexagonal channel for the Eu^{2+} dopant, coordinated by nine (N,O) atoms.[14–16] However, it was still absent of direct evidences to prove the precise microenvironment of Eu^{2+} in β-SiAlON. This fundamental question enables us to consider using the exhaustive photoluminescence measurements, such as high pressure and time-resolved spectroscopy, as an option to probe it.[15,16]

The luminescent properties of β-SiAlON:Eu are expected to be tuned by compositional tailoring, as β-SiAlON is a solid solution β-$Si_{6-z}Al_zO_zN_{8-z}$ with z in the range of 0–4.2. Based on this, many efforts are devoted to the study of β-SiAlON:Eu.[17–24] When z is decreased, the emission peak wavelength exhibits a blue-shift, and the FWHM decreases. Also the thermal quenching resistance of β-SiAlON:Eu phosphor enhances and obvious sharp lines on emission band appears with the decrease of z. These phenomena have been observed by many researchers. However, no comprehensive explanation has been provided yet. Until now, the red-shift of emission band with increasing z was often explained as the result of increasing of electron–lattice coupling manifested by the increase of Stokes shift being dominant in its competition with the decrease of nephelauxetic effect. The broadening of Eu^{2+} emission spectra with increasing Al–O content was attributed to the inhomogeneous broadening caused by higher disorder and less rigidity in the crystal structure.[8,11,19] Real and direct evidences are needed to prove these standpoints. Sharp-line fine structure in photoluminescence emission and excitation spectra of β-SiAlON:Eu have been observed by Takahasi *et al*.[20] at low temperature. However, the origin of the lines with higher energy than the assigned zero-phonon line are not discussed in-depth.

Herein, we demonstrate the synthesis of green-emitting phosphors, β-SiAlON:Eu, with different z values using gas pressure sintering (GPS) method. The structures and photoluminescence properties of these oxynitride phosphors are explored and studied in detail. The bold viewpoint that ample microenvironment around Eu^{2+} existing in β-SiAlON is confirmed by low-temperature photoluminescence spectra under different excitation wavelengths and time-resolved luminescence spectra. The origin of weak electron–lattice interaction, which enables observation of the sharp-line fine structure in photoluminescence spectra of β-SiAlON:Eu, is explained by specific features of the two electrons attracted by Eu^{2+} occupying interstitial sites in the crystal structure. The charge state evolution of Eu is ascribed to the distortion of highly symmetric EuN_9 polyhedron and less rigidity of lattice with the increasing ratio of O/N, proven by Raman spectra, Debye temperature, and solid-state magic-angle-spinning (MAS) NMR data. Rigid and ordered structure is important to obtain the high thermal stability of phosphor. Obvious improvement in NTSC space has been obtained from the low z β-SiAlON:Eu phosphor. All these results provide new insights for explaining the reason for narrow-band-emission in β-SiAlON:Eu and will deliver an impetus for exploring other narrow-band emitting phosphors.

2. EXPERIMENT SECTION

2.1. Synthesis of materials. β-$Si_{5.82}Al_{0.18}O_{0.18}N_{7.82}$:Eu (denoted as β-SiAlON:Eu (540)) with $z = 0.18$ was synthesized by high-pressure solid-state method using α-Si_3N_4 (SN-E10, Ube Industries, Japan), AlN (Type F, Tokuyama Corp., Japan), Al_2O_3 (Taimei Chemicals Co. Ltd., grade TMDAR), and Eu_2O_3 (Shin-Etsu Chemical Co. Ltd, Japan) as starting materials. Considering the phase stability in previous works,[7,11,19] the Eu concentration was set at 0.02 mol%. The precursors were weighed according to the stoichiometric ratio and thoroughly ground in the argon-filled glovebox ($H_2O < 1$ ppm, $O_2 < 1$ ppm). The powder mixture was transferred into boron-nitride (BN) crucibles and then sintered in a gas pressure sintering furnace (GPS, FVPHP-R-5, FRET-25, Fujidempa Kogyo Co. Ltd) with a graphite heater through one-step sintering method. The powder mixture was heated from room temperature (RT) to 1200 °C with a heating rate 10 °C/min under a vacuum of 10^{-2} Pa. High-purity (5N) nitrogen gas was introduced into the chamber to a pressure of 1.0 MPa at 1200 °C. The sintering temperature was increased to 1980 °C at a heating rate of 5 °C/min under 1.0 MPa N_2 atmosphere. Then the sample was fired at 1980 °C for 8 h. Finally, the product was powdered for further characterization. β-$Si_{5.97}Al_{0.03}O_{0.03}N_{7.97}$:Eu (denoted as β-SiAlON:Eu (529)) with $z = 0.03$ was prepared via a similar method using high-purity (4N) Si powder (Shin-Etsu Chemical Co. Ltd, Japan), AlN (Type F, Tokuyama Corp., Japan) and Eu_2O_3 (Shin-Etsu Chemical Co. Ltd, Japan) as starting materials. Considering the phase stability in previous works,[7,11,19] the Eu concentration was set at 0.33 mol%. The starting solids were weighed and ground in the argon-filled glovebox ($H_2O < 1$ ppm, $O_2 < 1$ ppm). Then, the powder mixture was transferred into BN crucibles and fired in the GPS furnace (FVPHP-R-5, FRET-25, Fujidempa Kogyo Co. Ltd) with a graphite heater via a two-step sintering method. In the first step, the sample was heated up to 800 °C in a vacuum of 10^{-2} Pa with a heating rate of 500 °C/h. High-purity (5N) nitrogen gas was introduced into the chamber to a pressure of 0.5 MPa at 800 °C. Then, the temperature was increased from 800 °C to 1300 °C with a heating rate of 500 °C/h. From 1300 °C to 1600 °C, the sample was heated up to 1600 °C with a slow heating rate of 1 °C/min and the temperature was maintained at 1600 °C for 8 h to make the Si powder completely nitrided. The sintered sample was ground into fine powder. With this, the first step was finished. In the second step, the sample was heated from RT to 2000 °C at a heating rate of 500 °C/h under 1.0 MPa N_2 atmosphere. The sample was fired at 2000 °C and kept for 8 h. Finally, the product was ground to powder for further characterization.

2.2. Characterization methods. Powder X-ray diffraction was performed on a Bruker D2 Phaser with CuKα radiation (λ = 1.5405 Å) at 30 kV and 30 mA. The neutron powder diffraction (NPD) data of these phosphors were collected using the high-resolution neutron powder diffractometer, ECHIDNA, at the Open Pool Australian Light-water (OPAL) research reactor, at the Australian Nuclear Science and Technology Organisation (ANSTO).[25] The NPD data were collected in the range of 6.50°–163.95° with a step size of 0.125°. Refinements of the structural analysis were executed using TOPAS 4.2 software. The wavelength of neutron was refined to be 1.621926(1) Å using the $La^{11}B_6$ NIST standard reference material (SRM) 660b. The compositions of the samples were determined using ICP-OES (Agilent 725-ES ICP-OES, USA). The morphologies of the as-prepared samples were observed using scanning electron microscopy (SEM, Nova NanoSEM 450, FEI, Oregon, USA).

Transmission electron microscopic (TEM) images, selected area electron diffraction (SAED) patterns, and high-resolution TEM (HR-TEM) images were recorded with a Jeol JEM-2011 electron microscope operated at 200 kV at the University of St Andrews, St Andrews, KY16 9ST, United Kingdom. The particle size data was collected using the Multisizer 3 (Beckman Coulter) particle size analyzer. The photoluminescence excitation (PLE) and emission (PL) spectra within the temperature range of 3–300 K were obtained with an Edinburgh FLS920 combined fluorescence lifetime and steady state spectrometer equipped with a 450 W Xe lamp and thermoelectric cooled red sensitive PMT. The room temperature luminescence decay curves of the as-prepared samples were also recorded on FLS920 equipped with a 150 W nF900 nanosecond flash lamp with a pulse width of 1 ns and a pulse repetition rate of 40 kHz. In addition, the steady-state photoluminescence measurements at 10–300 K were also recorded with an Andor SR-750-D1 spectrometer, equipped with a CCD camera DU420A-OE type. A He–Cd laser and semiconductor lasers were used as the excitation source. The experimental setup for the luminescence kinetics and time-resolved spectroscopy consists of a PL 2143 A/SS laser pumping a PG 401/SH parametric optical generator that generates 30 ps pulses of tuned wavelength with a frequency of 10 Hz. The detection part consists of a 2501S (Bruker Optics) spectrograph and a Hamamatsu C4334-01 Streak Camera. Time-resolved luminescence spectra were obtained by integration of the streak camera images over time spacing, whereas luminescence decays were gathered through the integration of the streak camera images over the wavelength intervals. All samples were cooled in a closed-cycle optical cryostat, and the temperature was allowed to vary from 10 K to 300 K. The system consists of a water-cooled He compressor model ARS-$_4$HW and expander model DE-204 SI manufactured by Advanced Research System, Inc. and LakeShore temperature controller Model 336. The Merrill Bassett type of diamond anvil cell is used for high pressure measurements. The culet diameter was 0.6 mm, and the sample chamber was a hole of approximately 0.2 mm in diameter drilled in an Inconel gasket. Polydimethylsiloxane oil was utilized as a pressure-transmitting medium. The standard ruby (Al_2O_3:Cr^{3+}) fluorescence technique was used to monitor pressure. The temperature-dependent (298–573 K) emission spectra were obtained by FluoroMax-3 spectrophotometer set up with a 150 W Xe lamp and Hamamatsu R928 photomultiplier tube equipped with the THMS-600 heating equipment. The absolute photoluminescence quantum yield was determined with QY C11347 (Hamamatsu). The vacuum ultraviolet (VUV) optical properties were measured at the temperature range of 10–300 K using the BL03A beamline coupled to 1.5 GeV storage ring at National Synchrotron Radiation Research Center (NSRRC) in Taiwan. The PLE spectra of the samples collected in the range of 100–350 nm were recorded by scanning a 6 m cylindrical grating monochromator with a grating of 450 grooves/mm. To remove the high-order light from the VUV synchrotron, a LiF plate was used as a filter. The PL emissions of the samples were analyzed with a 0.32 m monochromator and detected with a photomultiplier (Hamamatsu R943-02) in a photon-counting mode. The sample holder was attached to a a cold-head of a helium closed-cycle cryostat system (APD HC-DE204S); by this means, the temperatures of samples could be regulated in the range 10–300 K. The Eu L_3-edge X-ray absorption near-edge structure spectra were obtained on transmission mode at BL17C beamline at NSRRC, Taiwan. Specific heat measurements was used thermal relaxation method by PPMS heat capacity option (Quantum Design Company). Raman spectra were recorded on a Horiba JobinYvon Lab Ram Aramis spectrometer with a He-Ne laser providing excitation light at 633 nm with 1200 l/mm grating. Solid-state nuclear magnetic resonance (NMR) of ^{27}Al and ^{29}Si spectra were recorded on a wide-bore 14.1-Tesla Bruker Avance III NMR spectrometer, equipped with a 4 mm double-resonance magic-angle-spinning (MAS) probe head. The Larmor frequency for ^{27}Al and ^{29}Si were 156.4 and 119.2 MHz, respectively. ^{27}Al spectra were collected after a selective pulse ($\pi/6$) of 1.0 μs with a spinning rate of 13.5 kHz and a recycle delay of 1 s. ^{27}Al chemical shift was referenced to 1 M aqueous $Al(NO_3)_3$. As for ^{29}Si spectra, a selective $\pi/4$ pulse of 2.5 μs was used for the excitation source with a spinning rate of 13.5 kHz and a recycle delay of 60 s.

2.3. LEDs fabrication and performance measurement. In packaging white LEDs devices, the as-synthesized β-SiAlON:Eu^{2+} phosphors and commercial red K_2SiF_6:Mn^{4+} phosphor (CN-KR630, China Glaze) were mixed with silicone resin B and silicone resin A (A : B = 1 : 2; wt%). After bubbles were removed, the mixture was dropped onto a blue chip and then thermally cured for 2 h at 150 °C in an oven. After packaging was completed, the white LEDs devices was measured using a spectrophotometer with integrated spheres (EVERFINE, PMS-80) under direct current forward-bias condition. NTSC space was calculted by the color coordinates of RGB after the white LEDs devices passing through the color filters (conventional commercial products).

3. RESULTS AND DISCUSSION

3.1 Structural characterization. Figure 1a shows the structural overview of the green phosphor β-SiAlON:Eu, where a highly rigid, condensed framework of corner-sharing $(Si,Al)(O,N)_4$ tetrahedra with hexagonal channels viewed along [001] is built. The degree of condensation k, denoted as the atomic ratio (Si,Al):(N,O), in β-SiAlON is 3/4, similar to β-Si_3N_4. Single-phase β-SiAlON can be also described by the formula $Si_{6-z}Al_z(O_yN_{6-y})(O_xN_{2-x})$,[26–29] with $x + y = z$, where (N,O)1 atoms occupying the *6h* sites and (N,O)2 atoms occupying the *2c* sites (Figure 1a). In this structure, Eu^{2+} locates itself in empty lattice points in the endless channel along the [001] direction with a coordination number of nine, forming three shorter Eu–N bonds and six longer Eu–N bonds in the first coordination zone (Figure 1b). The compositions of β-SiAlON:Eu (529) and β-SiAlON:Eu (540) were determined via the ratio of Si:Al:Eu using ICP-OES. The z and dopant content of Eu^{2+} were calculated to be z = 0.031(2) and 0.33(5) mol% for β-SiAlON:Eu (529), and z = 0.185(2) and 0.02(1) mol% for β-SiAlON:Eu (540). Both of the as-synthesized phosphors are in pure phase (Figure S1). SAED patterns with bright diffraction spots and lattice planes confirms the hexagonal structure and reveal high crystallinity of the two samples (Figure S2). The diffraction peaks shift to lower angle due to the lattice expansion induced by Al–O content increases because the combination AlO^+ ($r(Al^{3+}) + r(O^{2-}) = 0.39 + 1.38 = 1.77$ Å) is larger than SiN^+ ($r(Si^{4+}) + r(N^{3-}) = 0.26 + 1.46 = 1.72$ Å) (Figure S1).[27] The crystallographic data refined from NPD data are shown in Figure 1c,d and summarized in Table S1. The obtained reliability factors R_{wp}, R_p, and x^2 all imply a good fitting quality and no secondary phase was detected. Meanwhile, the refined NPD data also indicate that O shows an overwhelmingly preferential oc-

cupation of the N2 (2c sites), in line with the result of the literature[14]. This occurrence provides abundant microenvironment around Eu^{2+} with different ratios of O/N in the second coordination zone (Figure S3). With increasing *z* value, the variety of microenvironment is expected to increase. As for a fixed *z* compound, a probability distribution of Eu@N1@(N,O)2 exists. With increasing substitution of Si–N by Al–O in *β*-SiAlON, a new probability distribution including more possibilities is characterized by different parameters values. The tunable luminescence properties induced by the substitution of Si–N by Al–O can be related to the evolution of this distribution.

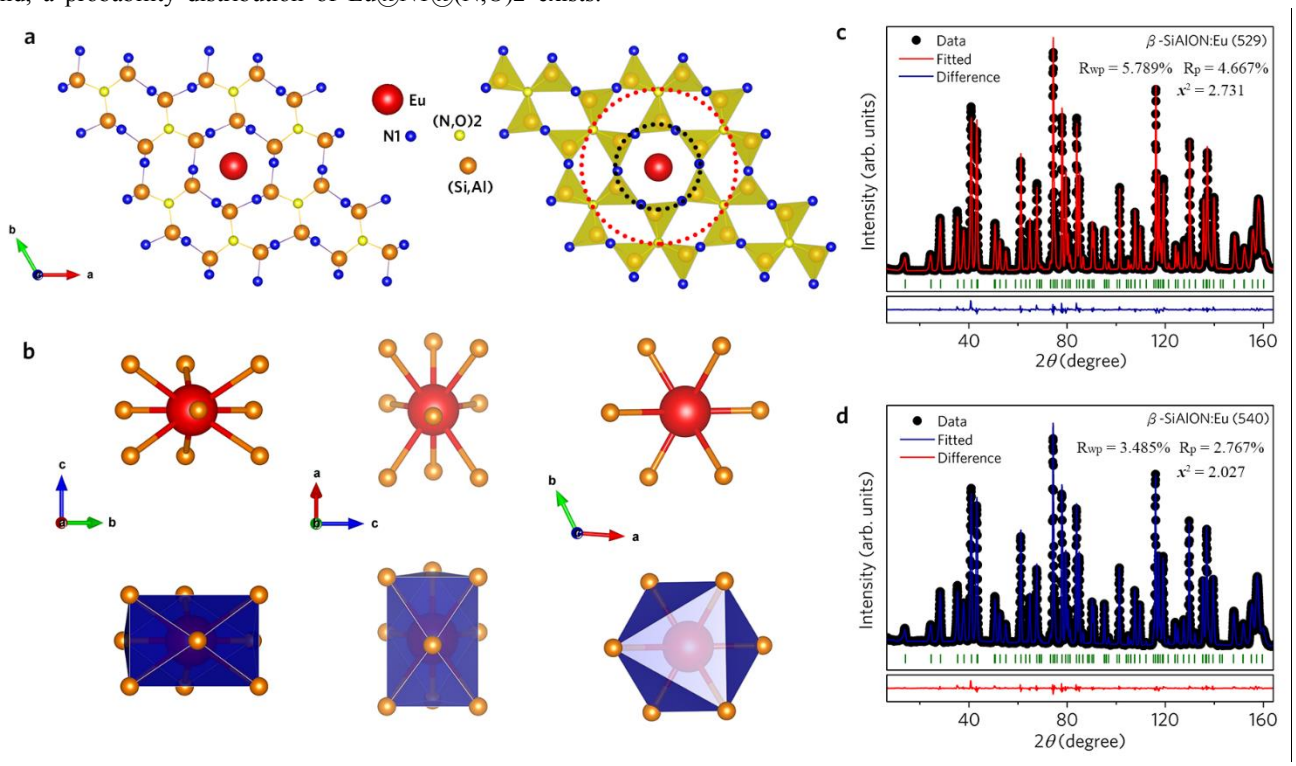

Figure 1. (a) Crystal structure of 2 × 2 × 2 unit cells of *β*-SiAlON:Eu viewed along *c*-direction. (b) Highly symmetric EuN_9 polyhedron viewed in *a*-, *b*-, and *c*-direction. Rietveld-fit profiles of neutron diffraction data for (c) *β*-SiAlON:Eu (529) and (d) *β*-SiAlON:Eu (540) oxynitride phosphors.

3.2. Unusual photoluminescence properties of *β*-SiAlON:Eu. The photoluminescence excitation and emission spectra of *β*-SiAlON:Eu (529) and *β*-SiAlON:Eu (540) are shown in Figure 2a. The observed emission spectrum of *β*-SiAlON:Eu (529) consists of a broad band peaked at 529 nm, assigned as transitions from the lowest $4f^6(^7F_J)5d^1$ (J = 0–6) state to the ground state $4f^7(^8S_{7/2})$ of Eu^{2+} ions, with some superimposed line structure. The observed fine structure at room temperature in the optical spectrum of Eu^{2+} in (oxy)nitride phosphors is a rare phenomenon. In contrast, the peak emission wavelength of *β*-SiAlON:Eu (540) is shifted to long wavelength (540 nm), and the line structure disappears. The excitation spectra of both samples consist of several overlapping bands located between 380 to 510 nm, indicating that these oxynitride phosphors can be used for UV or blue LED pumped illumination and display device. A surprising observation is that the maximum emission wavelength is shifted to a longer wavelength (red-shift) with increasing Al–O substitution. In general, the increased O/N ratio results in the reduction of the covalence of *β*-SiAlON, which normally cause a blue-shift of the emission band. Such an interpretation is in conflict with the red-shift phenomenon observed here. The red-shift in a given host depends on the downward shift of centroid, the strength of crystal field splitting of the 5d levels, and the value of Stokes shift. Generally, the centroid shift can be the result of the nephelauxetic effect, which depends on the binding strength of activator–ligand (Eu–N) in *β*-SiAlON:Eu. The covalency of the Eu–N bond is almost not affected by the adjacent O and Al atoms due to Eu occupying almost the same symmetrical EuN_9 polyhedron.[14] The magnitude of the crystal field splitting of 5d levels is sensitive to the shape and size of the local polyhedron, which can be further described by the average bond length (l_{av}) and distortion index (*D*) of the activator–anion polyhedron. Previous work has shown that a shorter l_{av} and a higher polyhedron distortion may increase the crystal field splitting. l_{av} were calculated to be 2.6778 and 2.6800 Å for *β*-SiAlON:Eu (529) and *β*-SiAlON:Eu (540), respectively. A polyhedral *D* can be calculated by:[30,31]

$$D = \frac{1}{n}\sum_{i=1}^{n}\frac{|l_i - l_{av}|}{l_{av}}$$

where l_i is the distance from the central atom to the *i*th coordinating atom and l_{av} is the average bond length. We found that *D* changes from 0.06723 to 0.06726 with an increase of Al–O (Figure 1c,d and Table S1). Typically, longer l_{av} leads to a small splitting, whereas larger *D* results in a larger splitting. To assess the dominating parameter, we calculated the percentage increase in l_{av} and *D* according to the method used by Wang[14] *et al.*. The results indicate that the percentage increase in l_{av} is 0.087%, which is larger than the increase in *D* (0.036%). This finding indicates that a blue-shift in emission. Moreover, such small changes in l_{av} and *D* are likely to play a negligible role in

the splitting of 5d energy levels, in line with the almost the same excitation spectra (Figure 2a and Figure S4). Therefore, we provide in this paper new insights to explain the red shift phenomenon in *β*-SiAlON:Eu with increasing *z* value. Under 460 nm excitation, the external (internal) quantum efficiency of green phosphor *β*-SiAlON:Eu (540) is measured to be close to 65 (82)%, which is higher than that of *β*-SiAlON:Eu (529) (36 (64)%). The reason is that the absorption efficiency of *β*-SiAlON:Eu (540) (79%) is higher than that of *β*-SiAlON:Eu (529) (56%) due to its larger particle size (Figure S5 and Figure S6). Moreover, the VUV photoluminescence properties at 10 K were studied for the first time and shown in Figure S7.

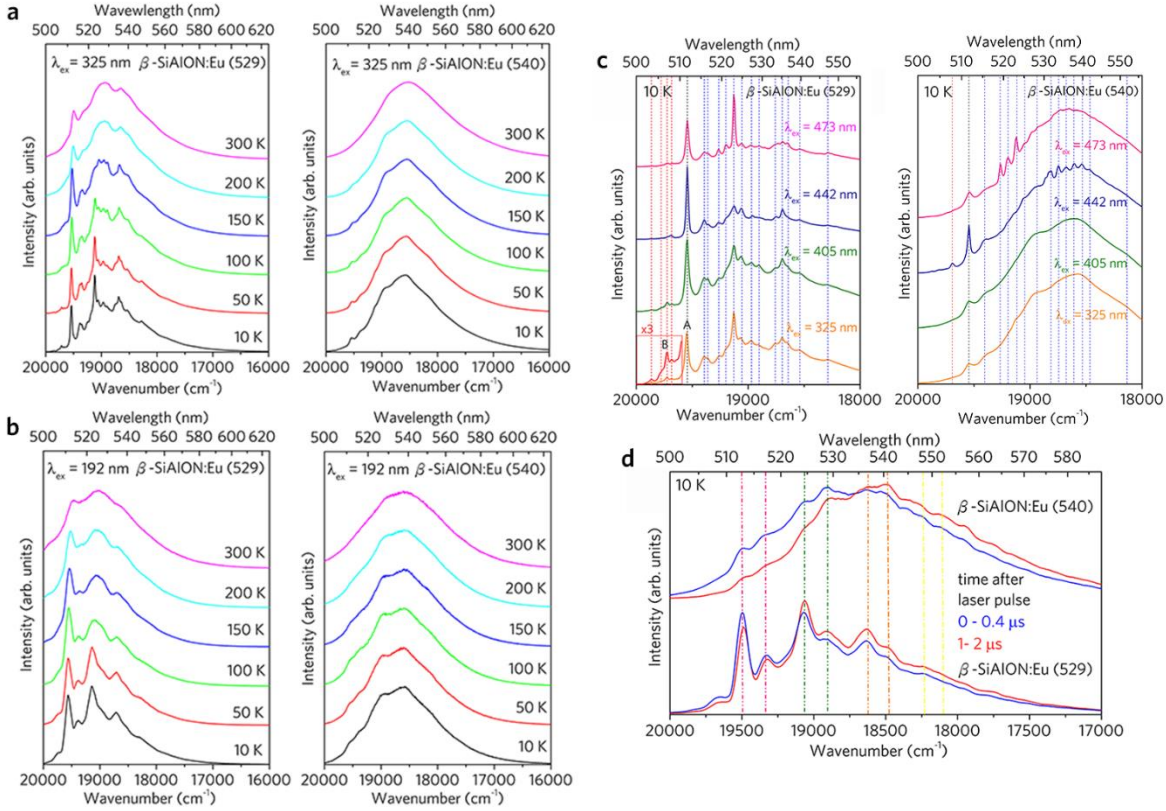

Figure 2. (a) Photoluminescence excitation and emission spectra of *β*-SiAlON:Eu (529) and *β*-SiAlON:Eu (540) green phosphors (dark arrows show the visible vibronic structure). (b) Excitation-wavelength-dependent emission spectra of *β*-SiAlON:Eu (529) and *β*-SiAlON:Eu (540) at 10 K. (c) Temperature-dependent emission spectra of *β*-SiAlON:Eu (529) and *β*-SiAlON:Eu (540) oxynitride phosphors under 325 nm excitation, respectively. (d) Time-resolved emission spectra of β-SiAlON:Eu (529) and β-SiAlON:Eu (540) under 325 nm excitation at 10 K.

3.3. Multi-microenvironment of Eu in *β*-SiAlON:Eu. To obtain more information on the structure observed in the emission spectra of *β*-SiAlON:Eu (529) and *β*-SiAlON:Eu (540), high-resolution emission spectra were recorded at 10 K (Figure 2b). Moreover, temperature-dependent emission spectra under 325 and 192 nm were determined (Figure 2c and Figure S8). The sharp-line fine structure of *β*-SiAlON:Eu (529) is better resolved by diminishing thermal broadening with the decrease in temperature. In the case of *β*-SiAlON:Eu (540), the spectrum also shows the sharp-line fine structure, but the individual lines are less resolved than that of *β*-SiAlON:Eu (529). Takahashi[20] *et al.* have already discussed this sharp-line fine structure of *β*-SiAlON:Eu with $z = 0.025$ and 0.24 at 6 K in detail. In the case of $z = 0.025$, the fine emission spectrum was ascribed to phonon-assisted transitions of single zero phonon line at 19607 cm^{-1} (510 nm), whereas for $z = 0.24$, the spectrum is complex and consists of a group of mutually shifted zero phonon lines and their associated phonon replicas. The fine excitation structure at 6 K was ascribed to Eu^{2+} ions that are ionically bonded with (N,O)1, and the Eu^{2+} excited state ($4f^6 5d$) is localized near the 4f orbital. This description of the photoluminescence properties presented in previous work[20] is, however, not comprehensive. For instance, it does not explain the origin of the sharp line (labeled as B in Figure 2b) with higher energy than the assigned zero phonon line A. This B line cannot be ascribed as an anti-stokes vibronic repetitions of zero phonon line A, because, at a temperature of 10 K, the thermal energy is too small to excite anti-stokes lines. Line B could be due to purely electronic transition (zero phonon line) of Eu^{2+} with different microenvironments.

To further observe the variation of emission band of *β*-SiAlON:Eu (529), we measured the excitation-wavelength-dependent emission spectra at 10 K. For both samples, the sharp-line fine structure is well resolved, complex, and depends on the excitation wavelength. Notably, for a given sample, the number of sharp lines and their positions do not depend on the excitation wavelength but the relative intensity of the individual peaks clearly varies. The change in relative intensity of the individual lines could be interpreted as a result of superposition of emission of the multi-microenvironment around Eu^{2+} with a different ratio of O/N, that is excited in a different manner depending on the excitation wavelength. The high energy part of the spectrum is enlarged in Figure 2b, revealing that a group of lines (at

least three lines) with higher energy than the identified zero phonon line A exists. To confirm this hypothesis, a careful measurement of the time-resolved luminescence was performed using the streak camera. The time-resolved spectra of *β*-SiAlON:Eu (529) and *β*-SiAlON:Eu (540) integrated over the 0 μs to 0.4 μs (blue curves), and 1 μs to 2 μs (red curves) time after a laser pulse are presented in Figure 2d. The spectral resolution of time-resolved measurement is lower than the steady state; thus, the individual lines overlap each other. In consequence, obtaining the exact decay time of individual lines is impossible. The Eu^{2+} luminescence decay curves were obtained for emission wavelength (1 nm spectral windows) marked with arrows in Figure S9 and respective decay times are presented in Table S2. Surprisingly, the decay time for each emission wavelength for both samples is different and increases monotonously with increasing monitored wavelength. This is inconsistent with the assumption that the observed lines are due to repetitions of single zero phonon line A. Under this assumption, one expects that the luminescence decay times of vibronic repetitions are the same as the decay time of zero phonon line. Experimental results cannot be explained even if we assure the presence of an additional zero phonon line at energies higher than line A. Under this assumption, one expects that the luminescence decay time of vibronic repetitions is the same as the decay time of zero phonon lines or it should fall between the decay times of zero phonon lines (in case of overlapping vibronic repetitions of different zero phonon lines).[32–37] Therefore, we postulate that an additional number of zero phonon lines with energies lower (and higher) than line A exists, each with a different decay time. Overlapping zero phonon lines and vibronic repetitions would lead to a different decay time observed at different wavelengths. In fact, because of a weak electron-lattice coupling of *β*-SiAlON:Eu (discussed below), we expect a very limited contribution of vibronic repetitions to the emission spectrum. In consequence, it may indicate that the majority of lines are due to purely electronic transitions (zero phonon lines) of the multi-microenvironment around Eu^{2+} with different atom ratio of O/N. However, some of lines observed in luminescence spectra are a result of vibronic assisted transitions. The Eu^{2+} microenvironments that are characterized by longer luminescence lifetimes are possibly characterized by larger electron–lattice coupling. In such a case, many lines observed at the lower energy are vibronic repetitions of the weak zero phonon lines.

The case of *β*-SiAlON:Eu (540) is similar to the *β*-SiAlON:Eu (529); the difference that is expected for *β*-SiAlON:Eu (540) is the enhancement of the variety of Eu^{2+} microenvironments due to the increased substitution of Si–N by Al–O. Figure 2b also shows the excitation-wavelength-dependent steady-state emission spectrum of *β*-SiAlON:Eu (540) at 10 K. The sharp-line fine structure of *β*-SiAlON:Eu (540) is not as well resolved as *β*-SiAlON:Eu (529) at 10 K. At the blue excitation wavelength (442 and 473 nm), Eu^{2+}, at a certain microenvironment is more selectively excited, which yields a more pronounced structure of the emission spectra in comparison with UV excitation (325 and 405 nm). Characteristic sharp photoluminescence lines of *β*-SiAlON:Eu (529) are also present for *β*-SiAlON:Eu (540) at the same positions (energies), indicating that the same microenvironments of Eu^{2+} are present in both samples. However, at the long wavelength part of the spectrum, new group of lines (excited at 442 nm), which presumably indicates the presence of a group of new Eu^{2+} microenvironments that are not present in *β*-SiAlON:Eu (529), are found. The intensity of the lines at the short wavelength part of the spectrum (high energy part) for *β*-SiAlON:Eu (540) are lower than intensities of respective lines for *β*-SiAlON:Eu (529). Simultaneously, decay curves for a short wavelength part of the *β*-SiAlON:Eu (540) emission spectrum are faster (and multi exponential) than the ones observed for *β*-SiAlON:Eu (529) (which are single exponential). Differences in spectral time evolution for both samples together with differences in the Eu^{2+} multi-microenvironment occupation are the possible reasons why emission band of *β*-SiAlON:Eu (540) is red shifted in comparison to *β*-SiAlON:Eu (529). An additional conclusion that can be drawn from Figure 2d is that *β*-SiAlON:Eu (540) contains the Eu^{2+} microenvironment presented in *β*-SiAlON:Eu (529) and additionally contains the Eu^{2+} microenvironment that are characterized by larger electron–lattice coupling and larger lifetimes not presented in *β*-SiAlON:Eu (529). This deduction is in accordance with the expected microenvironment around Eu^{2+} in *β*-SiAlON:Eu. An evident increase in luminescence decay time with an increase in monitored luminescence wavelength supports this conclusion.[37] In addition, the decay curves of *β*-SiAlON:Eu (529) and *β*-SiAlON:Eu (540) were also measured at RT (Figure S10 and Table S3). The obtained lifetimes show the same trend as that measured at 10 K. The decay time of the sharp lines as well as broad band for both samples are in the 0.6–1.2 μs range, which means that the observed luminescence is related to parity-allowed transitions from the excited states of electronic configuration $4f^6 5d^1$ to the ground state $^8S_{7/2}$ of $4f^7$ configuration of Eu^{2+}. The decay time of *β*-SiAlON:Eu (540) exhibits a larger range (0.64–1.17 μs) than that of *β*-SiAlON:Eu (529) (0.80–1.0 μs), which supports the probability distribution hypothesis of multi-microenvironment around Eu^{2+} with different O/N ratio.

3.4. Weak electron–lattice coupling induced by specific features of Eu occupying empty lattice points in the crystal structure. One should discuss the influence of electron–lattice coupling on the luminescence spectra of *β*-SiAlON:Eu. The configuration of the system of Eu^{2+} describes the ground $4f^7(^8S)$ state and the emitting state $4f^6 5d$. The six electrons from the $4f^6$ electronic configuration create the seven electronic levels: $^7F_0$–$^7F_6$, analogous to the Eu^{3+} which does not interact with the lattice ions since they are screened by $5s^2 5p^6$ electrons. Usually, a single 5d electron, interacts strongly with the lattice ions because it is located at a longer distance from the ion and is not effectively screened. Therefore, the excited electronic configuration $4f^6 5d$ is strongly coupled to the lattice. The respective situation is presented in the configurational coordinate diagram in Figure 3a,b. In this figure, the $4f^6(^7F_J, J = 0–6)5d$ electronic configuration and the ground state $4f^7(^8S_{7/2})$ are presented. The configurational space is represented by a single configurational coordinate *R*, which is proportional to the average distance between Eu^{2+} ion and ligands. The large electron–lattice coupling of the 5d electron is responsible for the splitting of the tenfold degenerated level and additionally causes the shortening of the Eu^{2+}-ligands bond lengths when the Eu^{2+} is excited to the lowest excited state of the $4f^6 5d$ electronic manifold as shown in Ref. 38,39 on the basis of ab initio theoretical studies for 4f→5d transition. This effect is responsible for diminishing the energy of the system in the excited state and is responsible for shifts of all excited states in the configurational space to lower values of *R*. The different spatial localizations of 4f and 5d electrons cause the $4f^6 5d$ state to retain much of the character of the 5d electron. Thus the absorption and emission transitions in single-electron approximation can be considered as 4f↔5d transitions.

The solid arrow represents the emission from the lowest state of the excited electronic configuration $4f^6(^7F_J, J = 0–6)5d$ to the ground state, which yields the broad band emission. The vertical dashed arrows represent the transitions to the excited electronic manifolds $4f^6(^7F_J, J = 0–6)5d$. For strong electron–lattice coupling of 5d electron both transitions are seen as broad bands and the individual transitions to the states $4f^6(^7F_0$ to $^7F_6)5d$ cannot be resolved (Figure 3a). When the interaction of 5d electron with lattice ions is sufficiently low (the weak electron–lattice coupling case) the shift of the $4f^6(^7F_0$ to $^7F_6)5d$ states with respect to ground state $4f^7$ ($^8S_{7/2}$) is small (see Figure 3b). In such a case, the transitions between the $4f^7 \rightarrow 4f^6 5d$ states in absorption and excitation spectra possibly retains the fine structure of the ^7F_J (J = 0–6) levels of $4f^6$ electronic configuration (see dashed arrows in Figure 3b). Also the luminescence is represented by zero phonon line and evident vibronic repetition (in Figure 3b only zero-phonon line is indicated by solid arrow). Such a fine structure in photoluminescence excitation spectrum was found in *β*-SiAlON:Eu, indicating that we deal with a weak electron–lattice coupling (Figure S4). To consider why the electron–lattice coupling of the 5d electron is weak, we should notice the peculiarities of the *β*-SiAlON:Eu system. In *β*-SiAlON crystal, unlike typical phosphors where Eu^{2+} substitutes lattice ion, the Eu^{2+} ions occupy interstitial sites. When Eu^{2+} occupies substitution sites (replaces Me^{2+} ions in the crystal structure), the charge neutrality requirement is satisfied and Eu^{2+} forms ionic bonds with negative ligand ions. The case when Eu^{2+} occupies the interstitial sites is different, because here Eu^{2+} provides additional positive charge which must be compensated. Therefore, to satisfy the charge neutrality requirement, Eu^{2+} attracts two electrons forming additional bonding-antibonding states[15,16]. If these two electrons are located between Eu^{2+} ion and ligand ions then can shield 5d electron in a manner similar to the $5s^25p^6$ shielding of the $4f^7$ electrons.[15] In consequence, the coupling of the 5d electron to the lattice can be strongly diminished. With the increase in *z*, the new microenvironments around Eu^{2+} with higher O/N ratio generate a higher disorder and less rigid structure, which causes an enhanced electron–lattice coupling. The red-shift of emission band as *z* increases supports this deduction.

The steady-state emission spectra of *β*-SiAlON:Eu (529) and *β*-SiAlON:Eu (540) obtained at 293 K under different pressures using 442 nm laser as excitation source are presented in Figure 3c,d. In Figure 3c, emission lines with numbers 1, 2 and 3 are indicated, which correspond to *β*-SiAlON:Eu (529) lines that are superimposed on the broad band spectrum. In Figure 3d, label 4 corresponds to the maximum of emission band of *β*-SiAlON:Eu (540). The individual lines with numbers 1 to 3 and maximum of emission band of *β*-SiAlON:Eu (540) (label 4) versus pressure are presented in Figure 3e. As the pressure increases, all the emission lines weakly shift towards lower energies. The red-shift of the emission lines 1 to 4 is similar. The respective rates range from 2 cm^{-1}/kbar to 2.4 cm^{-1}/kbar and are small, compared with the values of 10 cm^{-1}/kbar to 30 cm^{-1}/kbar observed for Eu^{2+} in other matrices.[40] The decrease in the energy difference between emitting excited state $4f^6 5d$ and ground state $4f^7$ is normally caused by increasing interactions of the emitting ion with its local environment due to decreasing inter atomic distances under pressure. To explain different shift rates under pressure, we have to take into consideration bulk modulus (which describes a volume change as a function of pressure and is constant for a given material) and the nature of states that are involved in the electronic transition. In the case of $4f^n \rightarrow 4f^n$ transition, the $4f^n$ electrons are shielded by the outermost $5s^25p^6$ electrons from interaction with lattice ions. In consequence, the observed pressure red shifts of $4f^n \rightarrow 4f^n$ transitions are small (approximately 1 cm^{-1}/ kbar to 4 cm^{-1}/ kbar). In the case of $4f^{n-1}5d^1 \rightarrow 4f^n$ transitions in Eu^{2+} ions, when Eu^{2+} occupies substitution sites, the 5d electron is not shielded and interacts strongly with lattice ions giving rise to observed red shift of $4f^6 5d \rightarrow 4f^7$ luminescence, an order of magnitude greater than $4f^n \rightarrow 4f^n$. The case when Eu^{2+} occupies the interstitial sites as described above is different; therefore, the red-shift of $4f^6 5d \rightarrow 4f^7$ Eu^{2+} luminescence in the case of *β*-SiAlON is extremely small. The small shift can also be related to rather large bulk modulus value (for *β*-Si_3N_4 is 2490 kbar) along with the shielding effect of attracted electrons. This result is in accordance with the proposed abovementioned model. After releasing the pressure, the emission spectra of *β*-SiAlON:Eu (529) and *β*-SiAlON:Eu (540) revert to their original profile and position, indicating that the emission of *β*-SiAlON:Eu is stable in all considered pressures.

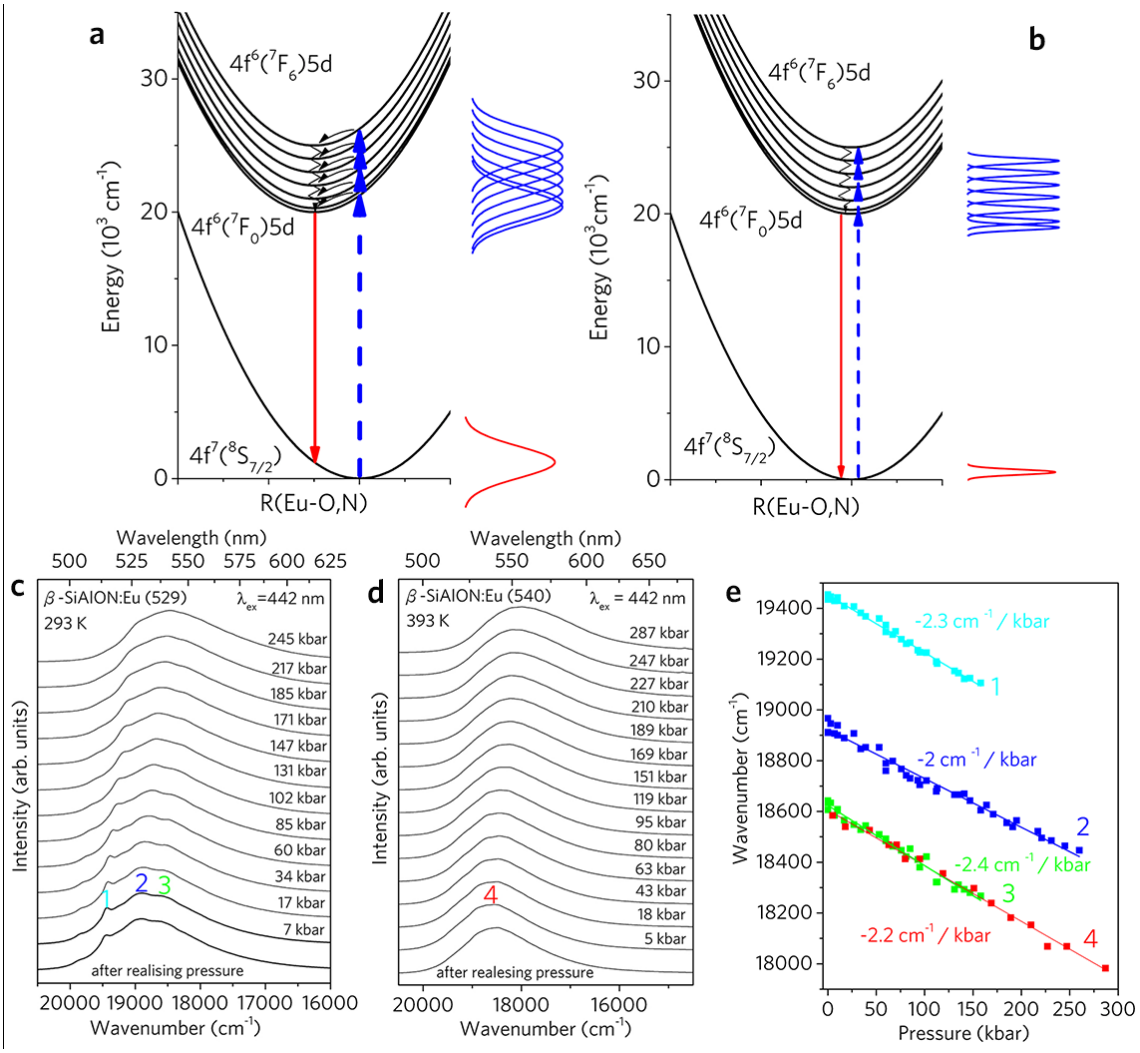

Figure 3. Configurational coordinate diagram representing the energetic structure of Eu^{2+} system for large (a) and small (b) electron –lattice coupling of the 5d electron with lattice, the respective emission and absorption line shapes are presented at the right side of the figures. (c,d) Luminescence spectra of β-SiAlON:Eu (529) and β-SiAlON:Eu (540) obtained for different pressure and (e) pressure shift of the individual lines marked in c and d.

3.5. Narrow-band-emission, high thermal stability, and charge state evolution of Eu induced by ordering structure in low z *β*-SiAlON:Eu. The thermal stability of luminescent material is vital in ensuring a high efficiency and stability of phosphor-converted devices. Figure 4a,b shows temperature-dependent photoluminescence spectra for *β*-SiAlON:Eu (529) and *β*-SiAlON:Eu (540). With the temperature varying from ambient temperature to 573 K, the peak intensity of both samples continuously decreases. In contrast, the emission intensity of *β*-SiAlON:Eu (540) decreases faster than that in *β*-SiAlON:Eu (529). The integrated intensity of *β*-SiAlON:Eu (540) also decreases with the increase of temperature, whereas *β*-SiAlON:Eu (529) shows an unusual trend. This difference is attributed to the obvious broadening of emission band, obscuring the sharp-line fine structure of *β*-SiAlON:Eu (529). The change in emission spectra with temperature between *β*-SiAlON:Eu (529) and *β*-SiAlON:Eu (529) is different from 298 K to 573 K, the peak wavelength and FWHM shifts from 528 nm and 49 nm to 538 and 69 nm for *β*-SiAlON:Eu (529). The peak wavelength and FWHM of *β*-SiAlON:Eu (540) shifts from 540 nm and 54 nm to 554 nm and 73 nm in the same temperature range. The shift of peak wavelength of *β*-SiAlON:Eu (529) is 352 cm^{-1}, which is smaller than that of *β*-SiAlON:Eu (540) (468 cm^{-1}) (Figure S11). The relatively larger ΔFWHM of *β*-SiAlON:Eu (529) is due to the sharp-line fine structure existing in emission spectra at room temperature. All the results demonstrate that *β*-SiAlON:Eu (529) shows better thermal stability than that of *β*-SiAlON:Eu (540). The origin of this difference is that the structure of *β*-SiAlON becomes soft and disorder, and the interaction between electron and lattice becomes obvious with increasing the Al–O content. The CIE shifts of *β*-SiAlON:Eu (529) and *β*-SiAlON:Eu (540) are also evaluated (Figure S11), which are lower than that of the red phosphors, such as $CaAlSiN_3:Eu^{2+}$ and $SrLiAl_3N_4:Eu^{2+}$.[41,42]

When Al→Si and O→N substitutions simultaneously occur in *β*-Si_3N_4, a structure of *β*-SiAlON is obtained, similar to that of *β*-Si_3N_4. As *z* increases, such substitution would inevitably cause an increasing degree of structural disorder in the framework of *β*-Si_3N_4, and consequently result in a decrease in the force constant of the Si–N bond. Reflected in the Raman spectra is the bands shift to lower frequencies and become broadening

with the increase of z.[28,43] Raman spectra of β-SiAlON:Eu^{2+} (529) and β-SiAlON:Eu^{2+} (540) are shown in Figure 4c. The positions of the peaks almost do not change, which indicates that the substitution content is very low. However, comparing with the data of β-SiAlON:Eu (529), the researchers found that the peaks become broader in β-SiAlON:Eu^{2+} (540). This result indicates that the structure becomes disorder when z increases. To obtain more information about local structure of β-SiAlON, NMR of ^{29}Si and ^{27}Al were used to study the local coordination and the results are shown in Figure 4d,e. The peak of ^{29}Si-NMR in both samples is located at -49 ppm, analogously to β-Si_3N_4. The difference is that the line width of β-SiAlON:Eu (540) is larger than that in β-SiAlON:Eu (529) but at the same time the line intensity β-SiAlON:Eu (540) is lower than that in β-SiAlON:Eu (529), which indicates that a small spread of bond lengths and angles in high z β-SiAlON:Eu structure. The ^{27}Al-NMR spectra show a distinct change in different z samples, associated with AlN_4 and $AlN_{4-x}O_x$.[44,45] This change demonstrates that the environment of Al becomes abundant, in accordance with the enhancement of the variety of the microenvironment around Eu^{2+}. The Debye temperature, Θ_D, is used as a proxy to quantify structural rigidity of a material, which can be experimentally determined by low temperature heat capacity (Figure 4f). The Θ_D can be extracted by fitting the heat capacity to the Debye model in the low temperature limit,[30,31]

$$C_P \approx \frac{12Nk_B\pi^4}{5}\left(\frac{T}{\Theta_D}\right)^3$$

where N is the number of atoms per formula unit multiplied by the Avogadro number, k_B is the Boltzmann constant, and T is the temperature. We find that the Θ_D of β-SiAlON:Eu (529) is 901 K, higher than that of β-SiAlON:Eu (540) (747 K). This result is consistent with the Raman data. The ordering and rigid structure of β-SiAlON with lower z strongly supports the enhanced thermal stability of β-SiAlON:Eu (529).[46] Meanwhile, The broaden and red-shifted emission of β-SiAlON:Eu with increasing the substitution of Si–N by Al–O can be logically explained by the number of microenviroment around Eu^{2+} ions increases, where the number of electronic transitions increases causing overlap, and the new emerging microenvironment of Eu^{2+} with disordering structure exhibits a stronger electron–lattice coupling.

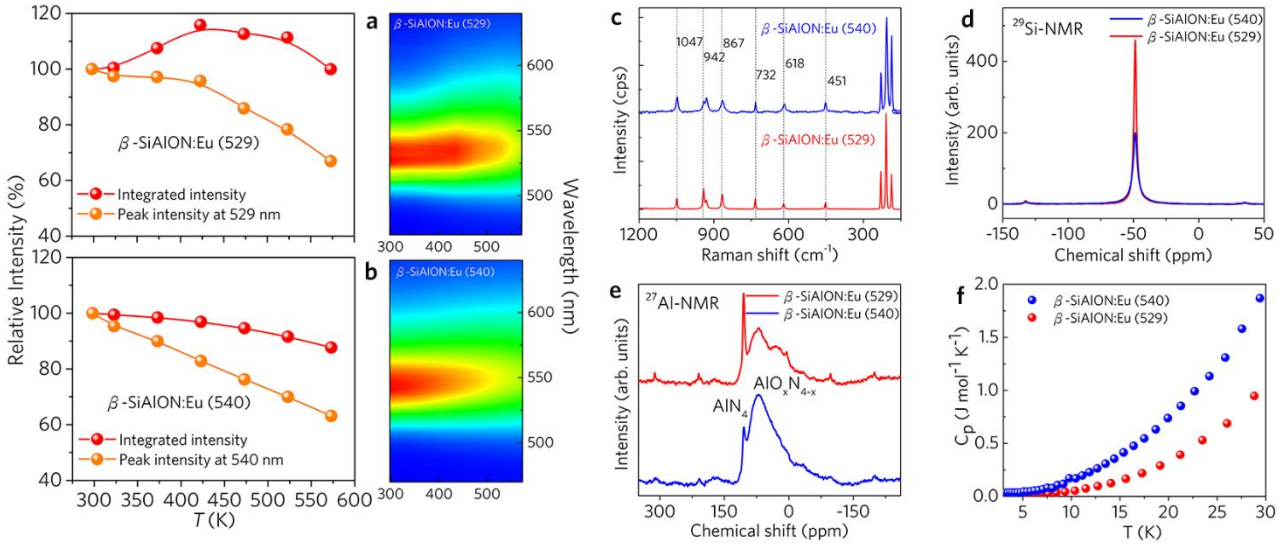

Figure 4. (a,b) Thermal quenching behavior of photoluminescence for β-SiAlON:Eu (529) and β-SiAlON:Eu (540); Temperature-dependent photoluminescence spectra are shown in the right-hand side. (c) Raman spectra, (d) ^{29}Si-NMR spectra, (e) ^{27}Al-NMR spectra and (f) low temperature heat capacity of β-SiAlON:Eu^{2+} (529) and β-SiAlON:Eu^{2+} (540).

X-ray absorption near-edge structure (XANES) spectroscopy was performed to determine the charge state of Eu in β-SiAlON:Eu (529) and β-SiAlON:Eu (540), and the results are shown in Figure 5a. $BaMgAl_{10}O_{17}$:Eu^{2+} and Eu_2O_3 are chosen as the standard Eu^{2+} and Eu^{3+}, respectively. The referenced Eu^{2+} peaked at 6974 eV, whereas the peak at 6984 eV ascribed to Eu^{3+}. The Eu L_3-edge XANES spectra of β-SiAlON:Eu (529) and β-SiAlON:Eu (540) reveal two peaks, which indicate that Eu^{2+} and Eu^{3+} coexist in both samples. The intensity of Eu^{2+} (inset of Figure 5a) is normalized to observe the ratio of Eu^{3+}/Eu^{2+}. This ratio is higher in β-SiAlON:Eu (540) than that in β-SiAlON:Eu (529), although the content of Eu in β-SiAlON:Eu (540) is lower than that in β-SiAlON:Eu (529). This phenomenon is attributed to the distortion of highly symmetric EuN_9 polyhedron and less rigidity of lattice with the increased Al-O substitution due to the longer bond lengths of Al–O (1.75 Å) compared with that Si–N (1.74 Å) along with all O atoms occupying (N,O)2 in β-SiAlON:Eu. Such a distortion of the highly symmetric EuN_9 polyhedron is suitable for Eu^{3+} due to the smaller radii of Eu^{3+} compared with that of Eu^{2+} with the same coordination number (see in Figure 5b). We further chose the characteristic excitation wavelength of Eu^{3+} to excite these phosphors, but only luminescence related to Eu^{2+} is observed (Figure S12). The results demonstrate that Eu^{3+} exists in both phosphors; however, it does not provide luminescence.[41,42]

3.6. White LEDs performance used in backlighting display. Benefitting from the narrower green-emitting of β-SiAlON:Eu (529), we fabricated white LEDs devices for backlight display by employing red emitter K_2SiF_6:Mn^{4+} (Figure 5c,d). Both white LEDs devices show the same color coordinates of (0.26,

0.23) and the same CCT of 33266 K. After went through the RGB color filters, the white LEDs device consisting of *β*-SiAlON:Eu (529) shows a 89% NTSC space, which means that the NTSC space obtained increased by 7% compared with the white LEDs device employing *β*-SiAlON:Eu (540). Moreover, we also compared the luminous efficacies and chromaticity of the fabricated white LEDs (Table S4). The luminous efficacy of the white LEDs with *β*-SiAlON:Eu (529) is 111 lm/W, less than that of the white LED using *β*-SiAlON:Eu (540) (128 lm/W), which is resulted from the lower EQE of *β*-SiAlON:Eu (529). In the future, the EQE of *β*-SiAlON:Eu (529) is expected to be improved by optimizing the synthesis condition using higher pressure and lower vacuum degree.

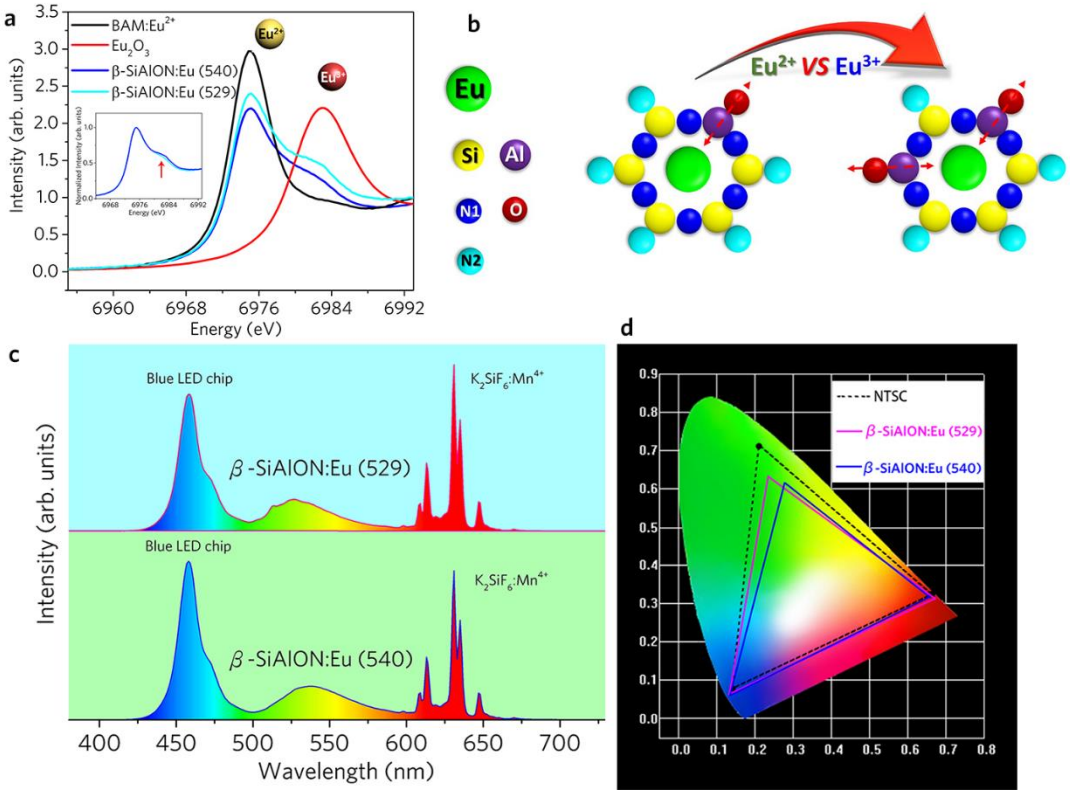

Figure 5. (a) Eu L_3-edge XANES spectra of *β*-SiAlON:Eu (529) and *β*-SiAlON:Eu (540). (b) Mechanism of Eu charge variation induced by Al–O substitution. (c) Electroluminescence spectra of LED devices consisting *β*-SiAlON:Eu (529) and *β*-SiAlON:Eu (540) phosphor, respectively, and (d) their NTSC spaces in CIE 1931.

4. CONLUSIONS

Excitation-wavelength-dependent emission spectra and luminescence kinetics at low temperatures were used as spectroscopic probes revealing the microstructure information around Eu^{2+} ions in *β*-SiAlON:Eu. Different from Eu^{2+} replacing ions in the crystal structure, in *β*-SiAlON:Eu phosphor, Eu^{2+} ions occupy the interstitial site. In such a case, Eu^{2+} attracts two electrons which should remain in the vicinity of Eu^{2+} forming additional bonding–antibonding states. These electrons can shield 5d electron in a manner similar to $5s^25p^6$ shielding the $4f^7$ electrons, proved as the high pressure photoluminescence. In consequence, the coupling of the 5d electron to the lattice is strongly diminished. The fine structure seen in excitation spectra is proof for that. The sharp-line fine structure of emission band in low *z* *β*-SiAlON:Eu is mainly attributed to the purely electronic transitions (zero phonon lines) of the multi-microenvironment around Eu^{2+} with different atom ratio of O/N. With the decrease in *z* value, the microenvironment around Eu^{2+} with lower O/N ratio becomes the dominant environment. Meanwhile, the structure of *β*-SiAlON becomes ordering and rigid. Attracted electrons by Eu^{2+} that are located between Eu^{2+} and ligands, shield 5d electron in a manner similar to $5s^25p^6$ shielding the $4f^7$ electrons, indicating that the effect of crystal field strength can be neglected. Therefore the enhanced rigidity and higher ordering structure of *β*-SiAlON:Eu became the main factors in the decrease of electron–lattice coupling with the decrease of *z*, which results in the blue-shift of the emission band and contributes to narrow emission band and charge state of Eu^{2+}. A prototype white LEDs employing narrower band emission *β*-SiAlON:Eu (529) as the green-emitting component shows an increase of 7% in NTSC space compared with the device using *β*-SiAlON:Eu (540). The main contribution of our results is providing new insights to reveal the link between the microenvironment of Eu, composition, and PL properties, able to initiate the exploration of narrow-band-emission phosphors with ordering structure and weak electron–lattice coupling.

ASSOCIATED CONTENT

Supporting Information

This material is available free of charge via the Internet at http://pubs.acs.org.

Figures S1–S12 and Tables S1–S4 (PDF)

AUTHOR INFORMATION

Corresponding Author

*Ru-Shi Liu. E-mail: rsliu@ntu.edu.tw Tel.: +886-2-33661169. Fax: +886-2-33668671.
*Agata Lazarowska. Email: a.lazarowska@ug.edu.pl Tel.: +48539983595.

Notes

The authors declare no competing financial interest.

ACKNOWLEDGMENT

The authors are grateful for the financial support of the Ministry of Science and Technology of Taiwan (Contract Nos. MOST 104-2113-M-002-012-MY3, MOST 104-2119-M-002-027-MY3 and 104-2923-M-002-007-MY3) and Australia Research Council (ARC, FT160100251). The contribution of A. L. was supported by the grant "Preludium" UMO-2014/13/N/ST3/03781 from the National Science Center. The contribution of S. M. was supported by the grant "Iuventus Plus" 0271/IP3/2015/73 from the Ministry of Science and Higher Education. M. G. was supported by Polish National Center for Research and Development with grants no PBS3/A5/48/2015 and PL-TWII/8/2015. We are also thankful to the staff members, especially Dr. Vanessa K Peterson, at the Australian Centre for Neutron Scattering, ANSTO for their operations support.

REFERENCES

(1) Pust, P.; Schmidt, P. J.; Schnick, W. A Revolution in Lighting. *Nat. Mater*. **2015**, *14*, 454–458**.**
(2) Xie, R. J.; Hirosaki, N.; Takeda, T. Wide Color Gamut Backlight for Liquid Crystal Displays using Three-Band Phosphor-Converted White Light-Emitting Diodes. *Appl. Phys. Express* **2009**, *2*, 022401.
(3) Pust, P.; Weiler, V.; Hecht, C.; Tücks, A.; Wochnik, A. S.; Henß, A.-K.; Wiechert, D.; Scheu, C.; Schmidt, P. J.; Schnick, W. Narrow-Band Red-Emitting $Sr[LiAl_3N_4]:Eu^{2+}$ as A Next-Generation LED-Phosphor Material. *Nat. Mater*. **2014**, *13*, 891–896.
(4) Xie, R.-J.; Hirosaki, N.; Li, Y.; Takeda, T. Rare-Earth Activated Nitride Phosphors: Synthesis, Luminescence and Applications. *Materals* **2010**, *3*, 3777–3793.
(5) Takeda, T.; Hirosaki, N.; Funahshi, S.; Xie, R.-J. Narrow-Band Green-Emitting Phosphor $Ba_2LiSi_7AlN_{12}:Eu^{2+}$ with High Thermal Stability Discovered by A Single Particle Diagnosis Approach. *Chem. Mater*. **2015**, *27*, 5892–5898.
(6) Strobel, P.; Schmiechen, S.; Siegert, M.; Tücks, A.; Schmidt, P. J.; Schnick, W. Narrow-Band Green Emitting Nitridolithoalumosilicate $Ba[Li_2(Al_2Si_2)N_6]:Eu^{2+}$ with Framework Topology whj for LED/LCD-Backlighting Applications. *Chem Mater.* **2015**, *27*, 6109–6115.
(7) Ryu, J. H.; Park, Y.-G.; Won, H. S.; Suzuki, H.; Kim, S. H.; Yoon, C. Luminescent Properties of β-SiAlON:Eu^{2+} Green Phosphors Synthesized by Gas Pressured Pintering. *J. Cera. Soc. Jap.* **2008**, *116*, 389–394.
(8) Niu, J.; Saito, G.; Akiyama, T. A New Route to Synthesize β-SiAlON:Eu^{2+} Phosphors for White Light-Emitting Diodes. *Appl. Phys. Express* **2013**, *6*, 042105.
(9) Liu, T.-C.; Cheng, B.-M.; Hu, S.-F.; Liu, R. S. Highly Stable Red Oxynitride β-SiAlON:Pr^{3+} Phosphor for Light-Emitting Diodes. *Chem. Mater.* **2011**, *23*, 3698–3705.
(10) Liu, L.; Xie, R.-J.; Hirosaki, N.; Takeda, T.; Zhang, C.-N.; Li, J.; Sun, X. Photoluminescence Properties of β-SiAlON:Yb^{2+}, A Novel Green-Emitting Phosphor for White Light-Emitting Diodes. *Sci. Technol. Adv. Mater.* **2011**, *12*, 034404.
(11) Ryu, J. H.; Park, Y.-G.; Won, H. S.; Kim, S. H.; Suzuki, H.;Yoon, C. Luminescence Properties of Eu^{2+}-Doped β-$Si_{6-z}Al_zO_zN_{8-z}$ Microcrystals Fabricated by Gas Pressured Reaction. *J. Cryst. Growth* **2009**, *311*, 878–882.
(12) Hirosaki, N.; Xie, R.-J.; Kimoto, K.; Sekiguchi, T.; Yamamoto, Y.; Suehiro, T.; Mitomo, M. Characterization and Properties of Green-Emitting β-SiAlON:Eu^{2+} Powder Phosphors for White Light-Emitting Diodes. *Appl. Phys. Lett.* **2005**, *86*, 211905.
(13) Kimoto, K.; Xie, R.-J.; Matsui, Y.; Ishizuka, K.; Hirosaki, N. Direct Observation of Single Dopant Atom in Light-Emitting Phosphor of β-SiAlON:Eu^{2+}. *Appl. Phys. Lett.* **2009**, *94*, 041908.
(14) Wang, Z.; Ye, W.; Chu, I.-K.; Ping Ong, S. Elucidating Structure-Composition-Property Relationships of the β-SiAlON:Eu^{2+} Phosphor. *Chem. Mater.* **2016**, *28*, 8622–8630.
(15) Mahlik, S.; Lazarowska, A.; Grinberg, M.; Liu, T.-C.; Liu, R. S. Luminescence Spectra of β-SiAlON/Pr^{3+} Under High Hydrostatic Pressure. *J. Phys. Chem. C* **2013**, *117*, 13181–13186.
(16) Lazarowska, A.; Mahlik, S.; Grinberg, M.; Liu, T.-C. ; Liu, R. S. New Pr^{3+} Site in β-SiAlON Red Phosphor. *Opt. Mater.* **2013,** *35*, 2001–2005.
(17) Takahashi, K.; Xie, R.-J.; Hirosaki, N. Toward Higher Color Purity and Narrower Emission Band β-sialon:Eu^{2+} by Reducing the Oxygen Concentration. *Electrochem. Solid-State Lett.* **2011**, *14*, 38–40.
(18) Zhu, X. W.; Masubuchi, Y.; Motohashi, T.; Kikkawa, S. The *z* Value Dependence of Photoluminescence in Eu^{2+}-Doped β-SiAlON ($Si_{6-z}Al_zO_zN_{8-z}$) with $1 \le z \le 4$. *J. Alloys Comp.* **2010**, *489*, 157–161.
(19) Xie, R.-J.; Hirosaki, N.; Li, H.-L.; Li, Y. Q.; Mitomo, M. Synthesis and Photoluminescence Properties of β-sialon:Eu^{2+} ($Si_{6-z}Al_zO_zN_{8-z}:Eu^{2+}$): A Promising Green Oxynitride Phosphor for White Light-Emitting Diodes. *J. Electrochem. Soc.* **2007**, *154*, 314–319.
(20) Takahashi, K.; Yoshimura, K.-I.; Harada, M.; Tomomura, Y.; Takeda, T.; Xie, R.-J.; Hirosaki, N. On the Origin of Fine Structure in the Photoluminescence Spectra of the β-sialon:Eu^{2+} Green Phosphor. *Sci. Technol. Adv. Mater.* **2012**, *13*, 015004.
(21) Gan, L.; Mao, Z.-Y.; Zeng, X.-H.; Zhang, Y.-Q.; Zhao, Y.; Xu, F.-F.; Zhu, Y.-C.; Liu, X.-J. The Origin of Bimodal Luminescence of β-SiAlON:Eu^{2+} Phosphors as Revealed by Fluorescence Microscopy and Cathodoluminescence Analysis. *Mater. Res. Bull.* **2014**, *51*, 205–209.
(22) Li, Y. Q.; Hirosaki, N.; Xie, R.-J.; Takeda, T.; Mitomo, M. Crystal and Electronic Structures, Luminescence Properties of Eu^{2+}-Doped $Si_{6-z}Al_zO_zN_{8-z}$ and $M_ySi_{6-z}Al_{z-y}O_{z+y}N_{8-z-y}$ (*M* = 2Li, Mg, Ca, Sr, Ba). *J. Solid State Chem.* **2008**, *181*, 3200–3210.
(23) Chung, J. H.; Ryu, J. H. Photoluminescence and LED Application of β-SiAlON:Eu^{2+} Green Phosphor. *Ceram. Int.* **2012**, *38*, 4601–4606.
(24) Kim, D.-H.; Ryu, J. H.; Cho, S.-Y. Light Emitting Properties of SiAlON:Eu^{2+} Green Phosphor. *Appl. Phys. A* **2011**, *102*, 79–83.
(25) Chen, C.-J.; Pang, W. K.; Mori, T.; Peterson, V. K.; Sharma, N.; Lee, P.-H.; Wu, S.-H.; Wang, C.-C.; Song, Y.-F.; Liu, R. S. The Origin of Capacity Fade in the $Li_2MnO_3{\cdot}LiMO_2$ (*M* = Li, Ni, Co, Mn) Microsphere Positive Electrode: An *operando* Neutron Diffraction and Transmission X-Ray Microscopy Study. *J. Am. Chem. Soc.* **2016**, *138*, 8824–8833.
(26) Loong C.-K.; Richardson, Jr. J. W. Crystal Phase and Phonon Densities of States of β-SiAlON Ceramics, $Si_{6-z}Al_zO_zN_{8-z}$ ($1 \le z \le 4$). *J. Am. Ceram. Soc.* **1996**, *79*, 3250–3256.
(27) Chen, W.-T.; Sheu, H.-S.; Liu, R. S.; Attfield, J. P. Cation-Size-Mismatch Tuning of Photoluminescence in Oxynitride Phosphors. *J. Am. Chem. Soc.* **2012**, *134*, 8022–8025.
(28) Boyko, T. D.; Gross, T.; Schwarz, M.; Fuess, H.; Moewes, A. The Local Crystal Structure and Electronic Band Gap of β-sialons. *J. Mater. Soc.* **2014**, *49*, 3242–3252.
(29) Okatov, S. V.; Ivanovskii, A. L. Chemical Bonding and Atomic Ordering Effects in β-SiAlON. *Int. J. Inorg. Mater.* **2001**, *3*, 923–930.
(30) Denault, K. A.; Brgoch, J.; Gaultois, M. W.; Mikhailovsky, A.; Petry, R.; Winkler, H.; DenBaars, S. P.; Seshadri, R. Consequences of Optimal Bond Valence on Structural Rigidity and Improved Luminescence Properties in $Sr_xBa_{2-x}SiO_4:Eu^{2+}$ Orthosilicate Phosphors. *Chem. Mater.* **2014**, *26*, 2275–2282.
(31) Denault, K. A.; Brgoch, J.; Kloβ, S. D.; Gaultois, M. W.; Siewenie, J.; Page, K.; Seshadri, R. Average and Local Structure, Debye Temperature, and Structural Rigidity in Some Oxide Compounds Related to Phosphor Hosts. *ACS Appl. Mater. Interfaces* **2015**, *7*, 7264–7272.
(32) Ryan, F. M.; Lehmann, W.; Feldman, D. W.; Murphy, J. Fine Structure in the Optical Spectra of Divalent Europium in the Alkaline

Earth Sulfates. *J. Electrochem. Soc.: SOLID-STATE SCIENCE AND TECHNOLOGY* **1974**, *121*, 1475–1481.
(33) Lizzo, S.; Velders, A. H.; Meijerink, A.; Dirksen, G. J.; Blasse, G. The Luminescence of Eu^{2+} in Magnesium Fluoride Crystals. *J. Lumin.* **1996**, *65*, 303–311.
(34) Kunkel, N.; Meijerink, A.; Kohlmann, H. Bright Yellow and Green Eu(II) Luminescence and Vibronic Fine Structures in $LiSrH_3$, $LiBaH_3$ and Their Corresponding Deuterides. *Phys. Chem. Chem. Phys.* **2014**, *16*, 4807–4813.
(35) Suta, M.; Wickleder, C. Photoluminescence of $CsMI_3:Eu^{2+}$ (M = Mg, Ca, and Sr) – A Spectroscopic Probe on Structural Distortions. *J. Mater. Chem. C* **2015**, *3*, 5233–5245.
(36) Meijerink, A.; Blasse, G.; Sytsma, J.; de Mello Donegá, C.; Ellens, A. Electron-Phonon Coupling in Rare Earth Compounds. *Acta Phys. Pol. A* **1996**, *90*, 109–119.
(37) Poort, S. H. M.; Meyerink, A.; Blasse G. Lifetime Measurements in Eu^{2+}-doped Host Lattices. *J. Phys. Chem. Solids* **1997**, *58*, 1451–1456.
(38) Barandiarán, Z.; Seijo, L. On the Bond Length Change upon $4f^1 \rightarrow 5d^1$ Excitations in Eightfold Coordination: $CaF_2:Ce^{3+}$ Cubic Defects. *Theor. Chem. Acc.* **2006,** *116*, 505–508.
(39) Barandiarán, Z.; Edelstein, N. M.; Ordejón, B.; Ruipérez, F.; Seijo, L. Bond Lengths of $4f^1$ and $5d^1$ States of Ce^{3+} Hexahalides. *J. Solid State Chem.* **2005**, *178*, 464–469.
(40) Liu R. S. *Phosphors, Up Conversion Nano Particles, Quantum Dots and Their Applications Volume 1*; Springer: Beijing, **2017**.
(41) Zhang, X.; Tsai, Y.-T.; Wu, S.-M.; Lin, Y.-C.; Lee, J.-F.; Sheu, H.-S.; Cheng, B.-M.; Liu, R. S. Facile Atmospheric Pressure Synthesis of High Thermal Stability and Narrow-Band Red-Emitting $SrLiAl_3N_4:Eu^{2+}$ Phosphor for High Color Rendering Index White Light-Emitting Diodes. *ACS Appl. Mater & Interfaces* **2016**, *8*, 19612–19617.
(42) Tsai, Y.-T.; Nguyen, H.-D.; Lazarowska, A.; Mahlik, S.; Grinberg, M.; Liu, R. S. Improvement of the Water Resistance of A Narrow-Band Red-Emitting $SrLiAl_3N_4:Eu^{2+}$ Phosphor Synthesized Under High Isostatic Pressure through Coating with An Organosilica Layer. *Angew. Chem.-Int. Edit.* **2016**, *33*, 9652–9656.
(43) Takase, A.; Tani, E. Raman Spectroscopic Study of β-sialons in the System Si_3N_4-Al_2O_3-AlN. *J. Mater. Sci. Lett.* **1984**, *3*, 1058–1060.
(44) Cozzan, C.; Griffith, K. J.; Laurita, G.; Hu, J. G.; Grey, C. P.; Seshadri, R. Structural Evolution and Atom Clustering in β-SiAlON: β-$Si_{6-z}Al_zO_zN_{8-z}$. *Inorg. Chem.* **2017**, *56*, 2153–2158.
(45) Bräuniger, T.; Kempgens, P.; Harris, R. K.; Howes, A. P.; Liddell, K.; Thompson, D. P. A Combined $^{14}N/^{27}Al$ Nuclear Magnetic Resonance and Powder X-Ray Diffraction Study of Imputy Phases in β-sialon Ceramics. *Solid State Nucl. Magn. Reson.* **2003**, *23*, 62–76.
(46) Brgoch, J.; Gaultois, M. W.; Balasubramanian, M.; Page, K.; Hong, B.-C.; Seshadri, R. Local Structure and Structural Rigidity of the Green Phosphor β-SiAlON:Eu^{2+}. *Appl. Phys. Lett.* **2014**, *105*, 181904.

“For Table of Contents Only”